Laser processing of freeform surfaces

Batal, Afif; Michalek, Aleksandra; Penchev, Pavel; Kupisiewicz, Axel ; Dimov, Stefan

DOI:
10.1016/j.ijmachtools.2020.103593

Document Version
Peer reviewed version

Citation for published version (Harvard):
Batal, A, Michalek, A, Penchev, P, Kupisiewicz, A & Dimov, S 2020, 'Laser processing of freeform surfaces: a new approach based on an efficient workpiece partitioning strategy', *International Journal of Machine Tools and Manufacture*. https://doi.org/10.1016/j.ijmachtools.2020.103593

Laser processing of freeform surfaces: A new approach based on an efficient workpiece partitioning strategy

A. Batal[1]✉, A. Michalek[1], P. Penchev[1], A. Kupisiewicz[2], S. Dimov[1]

[1] Department of Mechanical Engineering, University of Birmingham, Edgbaston, Birmingham, B15 2TT, UK
[2]Lasea SA, Liege Science Park, 4031 ANGLEUR, Belgium

Abstract

A novel method for laser processing freeform surfaces is proposed and demonstrated in this article. The method employs empirical data on the 3D limitations of a given laser process, namely the negative effects of focal offset and angle of incidence on the process performance, to partition a freeform surface into triangular laser processing fields. In this way, processing efficiency can be maximized by minimizing part repositioning while fully utilizing the capabilities of high dynamics galvo scanners. In this proof of concept, the surface of 3D printed Ti-6Al-4V spherical shells was improved by more than 90% and subsequently textured, using the proposed method. Conclusions were made about the advantages of this new approach for processing freeform surfaces consistently and efficiently.

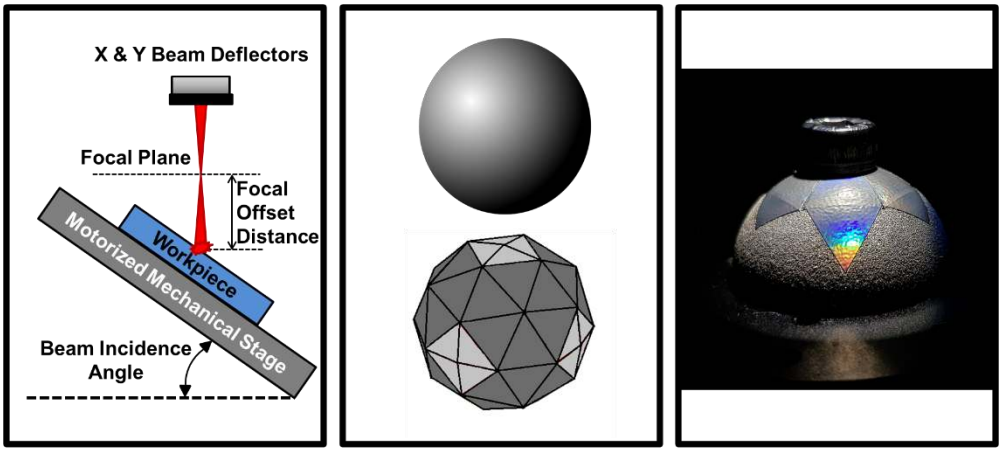

Keywords: 3D laser processing; freeform surface; surface partitioning; laser polishing; laser texturing; additive manufacturing

Nomenclature

Acronym	Definition
LPBF	Laser Powder Bed Fusion
AM	Additive Manufacturing
LST	Laser Surface Texturing
LIPSS	Laser Induced Periodic Surface Structures
LP	Laser Polishing
FOD	Focal Offset Distance
BIA	Beam Incidence Angle
FoV	Field of View

1. Introduction

Laser-based Powder Bed Fusion (LPBF) is a widely used additive manufacturing (AM) technology, commonly referred to as 3D printing, for producing near net shape engineering components. In the last decade LPBF has become a viable technology for a range of biomedical applications, more specifically in orthopedics, where it allows patient-specific and intricate designs with different mechanical and biological properties to be manufactured [1, 2]. One of the major shortcomings of LPBF technology is the surface integrity of the produced components, namely the resulting residual stresses and surface roughness, that have to be improved through post processing operations [3].

Titanium alloys are commonly used to produce biomedical implants and their mechanical polishing is undesirable due to their low thermal conductivity, high chemical reactiveness, high hardness and shear strength that lead to high tool wear and low processing rates [4-6]. Furthermore, custom tools and fixtures would be required to polish uniformly all functional surfaces of complex components. A promising alternative for finishing 3D printed components is laser polishing (LP) technology. In particular, the technology is a non-contact method, capable of processing freeform surfaces while retaining the geometrical accuracy obtained with the AM process. Furthermore, it is more environmentally friendly technology than commonly used chemical polishing processes.

Laser surface texturing (LST) as a technology for functionalizing surfaces was extensively investigated by researchers [7]. In the context of orthopedic applications, LST was shown to improve the performance of implants, namely by enhancing their biocompatibility and also by strengthening their mechanical bond with bones [8, 9]. Laser induced periodic surface structures (LIPSS) in particular offer some appealing opportunities for enhancing the performance of biomaterials. They are a regular ripple pattern that can be generated on almost any material when the laser intensity is at or near the damage threshold of the target material. Their periodicity is usually just under the wavelength of the laser source. LIPSS generation is generally attributed to some sort of interference between the incident laser beam and the surface-scattered electromagnetic waves [10, 11]. Their sub-micron length scale offers advantageous interactions with bone cells [12, 13].

Most laser surface processing research was conducted on planar substrates, however, processing disturbances are present when processing complex shapes, such as the acetabular shells found in total hip replacements [14]. This spherical component can be produced to near net shape by LPBF. The shells feature an outer surface that can benefit from some advantageous functional enhancements, such as anti-bacterial or osteoconductive properties, potentially offered by LIPSS, while their inner surface must be polished in order to minimize the wear of polyethylene liners. Thus, it would be beneficial, from a productivity standpoint, for both surfaces to be processed in one setup, particularly by employing LP on the inner surface and LP followed up by LST on the outer surface of the spherical shells. In this way, coatings and mechanical machining operations could potentially be avoided, they are currently required for their manufacture.

Both LP and LST were investigated extensively and proven on planar surfaces [5, 9, 15-17]. However, when laser processing 3D or freeform surfaces, they first have to be partitioned into fields while taking into account factors that affect the process uniformity and efficiency. In particular, variations in the beam incidence angle (BIA) and focal offset distance (FOD)

when processing 3D surfaces directly affect the process performance. Therefore, these two factors should be taken into account when deciding how to partition such surfaces for laser processing [14].

The most common approach to laser process complex geometries is to apply the so-called layered method. For instance, Yung et al. used a pulsed fiber laser to polish additively manufactured spherical CoCr alloy components by splitting them into layers, i.e. splitting the sphere in segments along its axis, and thus reducing surface roughness by up to 93% [18]. Other approaches for laser processing 3D parts include: the use of surface tessellation/triangulation algorithms for partitioning surfaces into planar fields and then using different scan-head positions for processing each of them [19]; layering the scanning fields of the focusing lens onto the freeform surfaces [20]; projecting 2D images onto 3D surfaces [21]; and also some combination of the aforementioned approaches [22]. Although, there were significant efforts dedicated to finding a generic solution to this complex problem, all available approaches still require some compromises to be made, for instance, not factoring the effects of both BIA and FOD when partitioning 3D surfaces, using a large number of scanning fields or a large number of different fields' geometries. Therefore, further efforts are required to address these open issues, especially to consider simultaneously the effects of both BIA and FOD and minimize part repositioning by setting 3D laser processing tolerances to obtain the overall desired process performance and productivity, using the smallest number of processing fields possible.

In this paper a method for laser processing complex 3D components is proposed that allows a higher processing efficiency to be achieved by maximizing the use of high dynamics galvo scanners and minimizing the number of processing fields all the while ensuring process performance. A pilot application of the proposed method is reported that demonstrates how different laser processing operations can be performed on 3D components, specifically, laser polishing and texturing was carried out on the surfaces of additively manufactured Ti-6Al-4V spherical shells.

2. Methodology for partitioning freeform surfaces

Contrary to conventional machining, such as milling, the laser beam does not need to be 'in-contact' with the workpiece. As such, laser processing setups and operations can tolerate some deviations in BIA from normal and also of some FOD before the process performance deteriorates. These intrinsic characteristics can be used advantageously through off-focus processing with varying BIA, and thus fully utilizing the high dynamics of beam deflectors while avoiding the need for constant refocusing. In addition, the use of relatively slow mechanical stages for part repositioning can be minimized by using as big as possible processing fields, and thus to increase the processing efficiency even further. However, the position of the scan-head relative to the working surface has an impact on process performance. Therefore, the effects of processing disturbances, i.e. deviations of the BIA from normal and off-focus processing, should be taken into account when processing strategies are designed, especially when partitioning 3D surfaces into laser processing fields [14]. A novel partitioning method is proposed in this research that employs an efficient strategy for tessellating 3D surfaces. The method is driven by predetermined 3D laser processing tolerances, i.e. max BIA and max FOD, to keep the process in control. In

particular, the geometrical parameters that are commonly used to control the tessellation in most CAD packages are set based on these 3D laser processing tolerances, in the proposed method.

2.1 Laser processing tolerances

The method requires the laser processing tolerances, i.e. the processing constraints associated with BIA and FOD, to be determined by conducting preliminary laser processing trials. Therefore, first, a laser processing operation, e.g. polishing, texturing or engraving, should be optimized on a planar substrate in 'ideal' conditions, i.e. in-focus (FOD = 0) and BIA normal to the surface, these processing parameters are then used as reference. Secondly, the effects of BIA and FOD on process performance should be investigated independently and quantified. Finally, cut-off values for BIA and FOD should be defined beyond which the process performance is no longer deemed satisfactory: they are referred to as processing tolerances in this research. The set of optimized processing parameters and processing tolerances, i.e. max BIA and max FOD, are specific for a given laser processing operation and substrate material. An example, how they can be obtained for a given laser processing setup, operation and material is provided in Section 3.

2.2 Surface tessellation

The surface tessellation process in the proposed method employs common algorithms available in most CAD packages and their respective set of geometrical parameters, i.e. the max edge length of a triangular field, the max chord height, and the tessellation angular tolerance. They are used to drive the partitioning process and, in the proposed method, are determined based on the 3D laser processing tolerances, i.e. the identified BIA and FOD constraints for a given laser processing setup, operation and material. They define the 3D laser processing strategy, especially by partitioning 3D surfaces into triangular fields that are then used to determine scan-head positions and fields for subsequent processing. In particular, the following three constraints should be considered when executing the surface tessellation process.

i. The field of view (FoV) of the used focusing lens introduces a constraint with regards to the size of the triangular fields. In particular, the longest side of any triangular field (max edge length) is determined by the focusing lens's FoV as follows:

$$max\ edge\ length \leq \sqrt{2}\ s \qquad (1)$$

where: s is the length of the FoV side as shown in Figure 1.

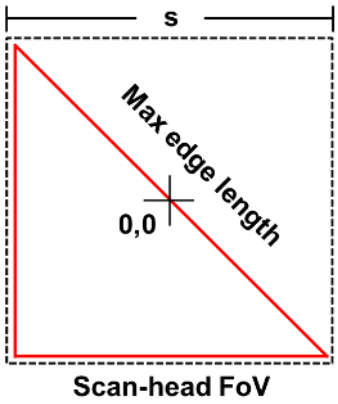

Figure 1. Triangle max edge length

Also, it should be noted that to make the best use of the available FoV for any given laser processing setup, the tessellation process should aim to generate triangular fields that are as close as possible to right-angle isosceles triangles, with a max edge length equal to the FoV diagonal as shown in Figure 1. Finally, the scan-head's (0,0) position should coincide with the triangle's circumcenter to meet the following processing tolerances.

ii. The processing tolerance defined by the FOD limit introduces a constraint on the maximum chord height in the tessellation process [23]. Especially, to keep the process in control the maximum chord height should not exceed twice the FOD limit, in particular:

$$max\ chord\ height\ \leq 2\ FOD\ limit \qquad (2)$$

In this way, the focal plane can be positioned halfway between the triangular field and the plane parallel to it that is also tangential to the 3D surface as shown in Figure 2. Thus, the depth of focus associated with any given laser processing setup will be fully utilized.

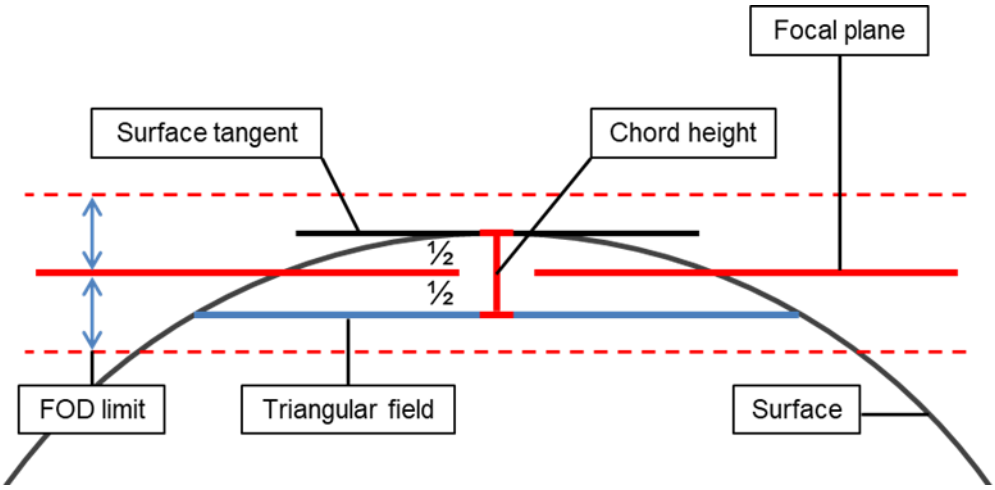

Figure 2. Tessellation max chord height

iii. The tessellation angular tolerance defined as the angle between the normal vectors of two adjacent triangles [24] should be constrained by the BIA limit. Particularly, the angle between surface tangents and the triangular fields, θ, does not exceed a given angular tolerance, α, when using STL tessellation algorithms [23]. Therefore, α can be used to control the BIA on the 3D part. If a telecentric focusing lens is used, α would be constrained by the BIA limit at the vertices of the triangular fields as shown in Figure 3a. However, when using the full FoV of F-Theta lenses, the lens's max deflection angle, β, should be also considered (Figure 3b) when defining a constraint for α. Especially, the relationships between θ, α and BIA limit in the case of telecentric lenses can be expressed as follows:

$$\theta \leq BIA\ limit \quad \text{and thus} \quad \alpha \leq BIA\ limit \qquad (3)$$

While in the case of F-Theta focusing lenses, the relationship will be:

$$\theta \leq BIA\ limit - \beta = BIA\ limit - \tan^{-1}\left(\frac{\sqrt{2}/2.s}{f}\right) \quad \text{and thus} \quad \alpha \leq BIA\ limit - \beta \qquad (4)$$

where: s is the lens FoV size and f its focal length.

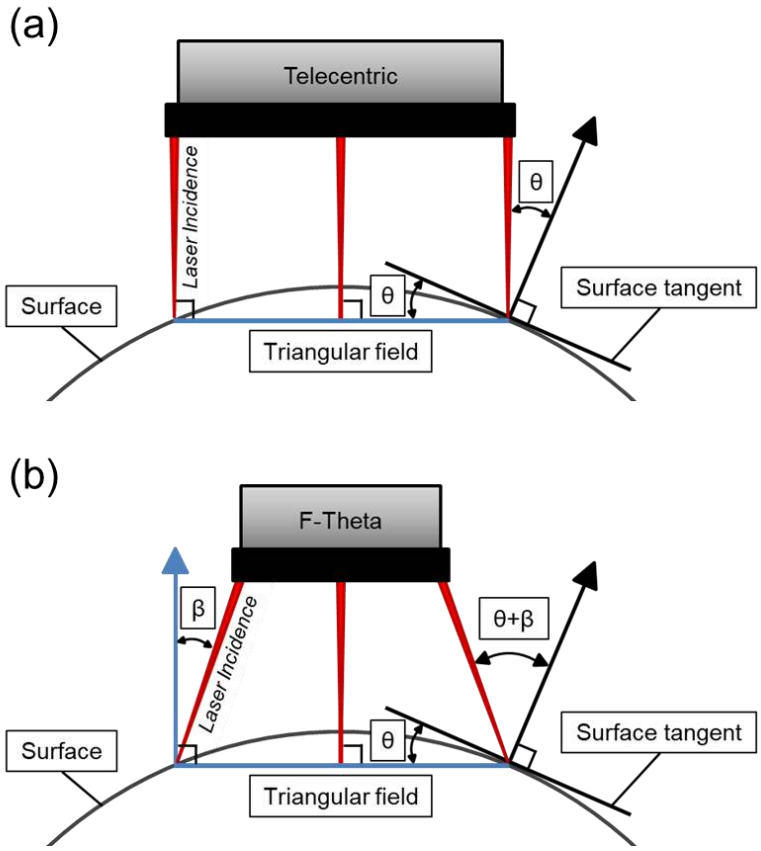

Figure 3. A schematic representation of BIA relative to the normal vectors and triangular fields in the case of (a) telecentric lenses and (b) F-Theta lenses.

2.3 Fields' distortion

Prior to laser processing the generated triangular fields onto the freeform surface, they must be, along with any feature they enclose, adjusted for any projection distortion. Essentially, the borders and any pattern or geometry inside the triangular fields must be projected onto the freeform surface (the triangles' vertices lie on the surface and therefore they would remain unchanged). This is necessary to make sure that the different fields stitch as required on the 3D surface and that patterns or structures are undistorted on the final part. The adjusted fields' borders or stitching areas would remain within the laser processing tolerances, because:

1) They lie between the between the triangular field and the plane parallel to it that is also tangential to the freeform surface. The fields' borders would essentially stay within the process's depth of focus.
2) The angle between the normal to the surface and the laser beam is smaller at the triangular fields' borders than at their vertices where it is highest.

The adjusted fields are effectively the inverse of the projections of the undistorted triangles onto the freeform surface as shown in Figure 4. As an example, the barrel and pincushion distorted triangular fields on the concave and convex surfaces are essentially the projections of an undistorted triangle from the projection plane (see Figure 4a), whereas the pincushion and barrel distorted triangles in the projection plane would be converted into undistorted triangular fields on the freeform surface (see Figure 4b).

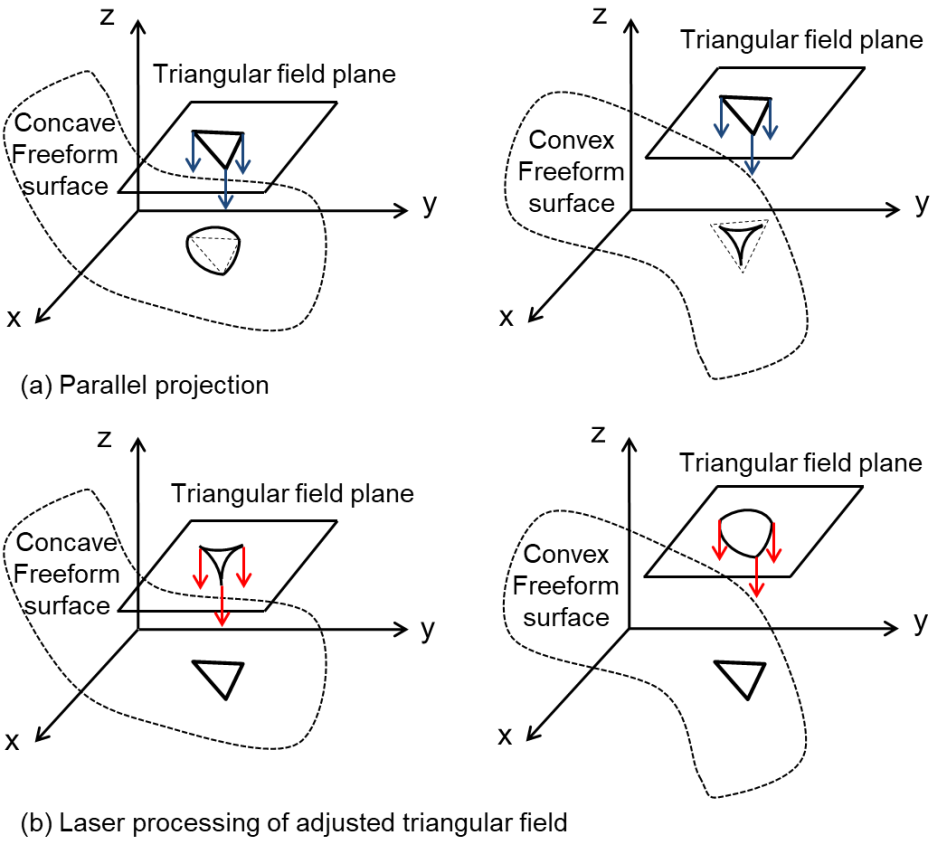

Figure 4. Schematic representations of projection distortions

2.4 Fields' overlapping

Finally, the projection-adjusted triangular fields may need to overlap when executing some laser processing operations, e.g. laser polishing, as it would be discussed in Section 4.2. If a given laser processing operations does not require any overlapping, regardless a small one should be introduced to compensate for any workpiece repositioning errors, e.g. because of some repeatability errors associated with the mechanical stages and/or beam deflectors. It is worth noting that the overlaps are introduced geometrically by proportionally extending the boundaries of the adjusted triangular fields along vectors originating at their centroids to maintain the overall field geometry as depicted in Figure 5. It should also be noted that the overlapping region does not necessarily satisfy the laser processing tolerances associated with FOD and BIA, as they are just extensions beyond the original bounds of the triangular fields. Therefore, a certain 'safety factor' should be used when setting the 3D processing tolerances to account for potential overlapping requirements, e.g. dictated by a specific laser processing operation or setup.

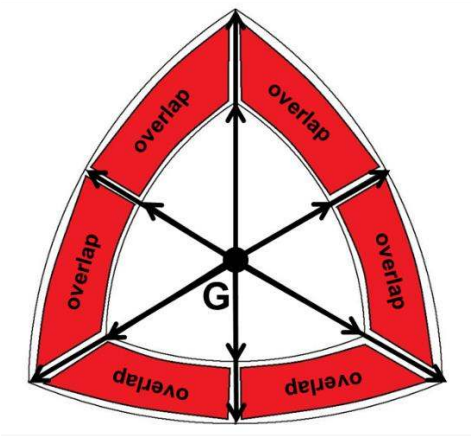

Figure 5. An example of boundaries' extension of a distortion-adjusted triangular field

3. Pilot implementation

A pilot implementation of the proposed methodology is presented in this section. Especially, as it was already mentioned in the introduction, it would be advantageous to perform multiple laser processing operations on acetabular shells found in total hip replacements. Therefore, a spherical component that resembles the functional surfaces of such shells was selected to demonstrate the capabilities of the proposed method. In particular, spherical shells produced to near net shape by LPBF were laser polished and textured by applying the proposed method, i.e. to partition their spherical surfaces for follow up laser processing. The conducted experimental study demonstrating the proposed surface partitioning/tessellation method is presented in this section.

3.1 Spherical shells produced by laser powder bed fusion

The spherical shells were built using a LPBF system, i.e. the RenAM 500M machine from Renishaw. The build parameters used to produce the shells were as follows: 200 W average laser power, 90 μm point distance (distance between 2 laser irradiation positions), 60 μs

exposure time, 90 µm hatch spacing and 30 µm layer thickness. The material used to build the shells was grade 23 Ti-6Al-4V, low interstitial.

The spherical shells were 30 mm in diameter with a thickness of 1 mm. An initial optimization of LP and LST processes, required for the implementation of the proposed methodology (see Section 2.1), was conducted on planar substrates. They were produced with the shells in the same build. The build direction for the planar samples was normal to the substrates and their surface roughness, i.e. initial arithmetical mean height (Sa) and root mean square height (Sq), were approximately 5.0 µm and 7.0 µm, respectively.

3.2 Laser polishing

The LP operation was optimized by conducting experimental trials using a MOPA-based Yb-doped fiber nanosecond laser source (SPI G4 50W HS-S) with the following technical characteristics: 50W average power, 0.71mJ maximum pulse energy, pulse duration from 15 to 220 ns, 1MHz maximum repetition rate, 1064 nm center wavelength and beam quality M^2 better than 1.3. The beam was focused using a telecentric lens with a 100mm focal length down to a spot size at the focal plane of approximately 40µm. Furthermore, the LP trials were carried out in a controlled Argon environment, flowing at 12L/min to maintain a positive pressure inside the chamber, in order to prevent surface oxidation and cracking [5, 25].

The LP parameters optimized by Ma et al. [5] on planar 3D printed Ti-6Al-4V substrates are provided in Table 1. They were used as a reference to study the effects of 3D laser processing disturbances on the LP performance. In particular, samples were processed in an inert gas-controlled environment using the LP settings in Table 1. The scan paths used were bidirectional with perpendicular and parallel tracks having the same stepover distance. The BIA and FOD values were varied independently and thus to investigate their effects on the surface roughness of LPBF Ti-6Al-4V substrates.

Table 1. Laser polishing parameters

Pulse Energy (µJ)	Pulse Duration (ns)	Pulse Repetition Rate (Hz)	Scanning Speed (mm/s)	Stepover Distance (µm)
80	220	500,000	200	16

3.3 Laser surface texturing

Laser sub-micron texturing was conducted using a femtosecond (fs) fiber laser (Satsuma from Amplitude Systemes) with the following technical characteristics: 5W average power, 10µJ maximum pulse energy, 310 fs pulse duration, 500 KHz maximum repetition rate, 1030 nm center wavelength and beam quality M^2 better than 1.2. The beam was focused using the same telecentric lens down to a spot size at the focal plane of 40 µm. The two laser sources used for the LP and LST operations were integrated into a Lasea LS5 system and the laser processing setup is illustrated in Figure 6.

LIPSS were used to texture the surfaces of laser polished Ti-6Al-4V substrates produced by LPBF. The parameters' domain for producing LIPSS is relatively big and therefore the LST parameter settings used in this research were selected based on a previously reported optimization study [14]. They are provided in Table 2. Again, as it was the case with the LP operation, planar Ti-6Al-4V substrates produced by LPBF and then laser polished with the

reference parameters in Table 1 were textured using the optimized LST parameters. These experimental trials were used to investigate the effects of FOD and BIA on the resulting sub-micron texture.

Table 2. Laser surface texturing parameters

Pulse Energy (µJ)	Pulse Duration (fs)	Pulse Repetition Rate (Hz)	Scanning Speed (mm/s)	Stepover Distance (µm)
2.8	310	250,000	1500	6

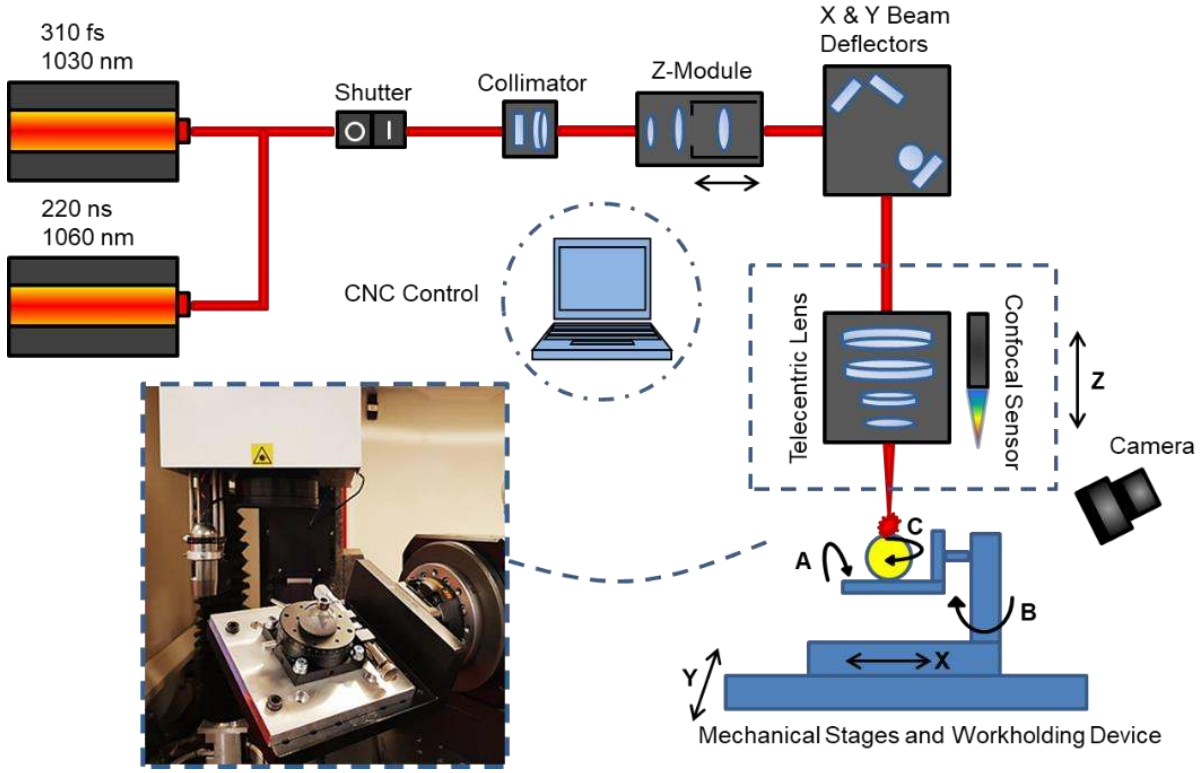

Figure 6. The used multi-axes laser processing setup

3.4 Partitioning of spherical surfaces for laser polishing and texturing

A triangulation algorithm based on the geometrical arrangements of geodesic polyhedra was used to tessellate the spherical surfaces, namely tetrahedra, octahedra and icosahedra arrangements were considered [26]. This algorithm is very efficient when applied on spheres as it generates the smallest number of triangular fields, for a given set of constraints, and the tessellation processes is very uniform. In particular, a very small number of different triangles are generated when tessellating a sphere, only 2 in this research as 2 subdivisions (3 frequencies) were examined for each of the 3 geometrical arrangements.

A MATLAB program was created for tessellating spherical surfaces that uses as inputs laser processing tolerances and the sphere diameter. The program tessellates spheres with the biggest possible triangles, hence generates as small as possible number of fields, with respect to a set of processing tolerances, i.e. max edge length, max chord height and the set

angular tolerance. Furthermore, the program applies the necessary corrections to account for any projection distortion and can add an optional overlapping between the fields to compensate for any workpiece repositioning errors as discussed in sections 2.3 and 2.4. It can serve as one-step solution for partitioning and fully pre-processing the CAD data necessary for laser processing spherical surfaces, and therefore avoiding the use of expensive CAD/CAM packages. The algorithm implemented into the MATLAB program is outlined in Figure 7.

The advantages of this partitioning method are highlighted in Figure 8. In particular, if a sphere with a 30 mm diameter is to be tessellated by using max chord height of 1.14 mm as a geometrical constraint, a common STL tessellation generated in PowerShape yielded 120 triangles with varying geometries while only 72 triangles of 2 different isosceles types would be generated using octahedron partitioning. Therefore, geodesic polyhedra arrangements are more effective in pre-processing spherical surfaces for laser processing.

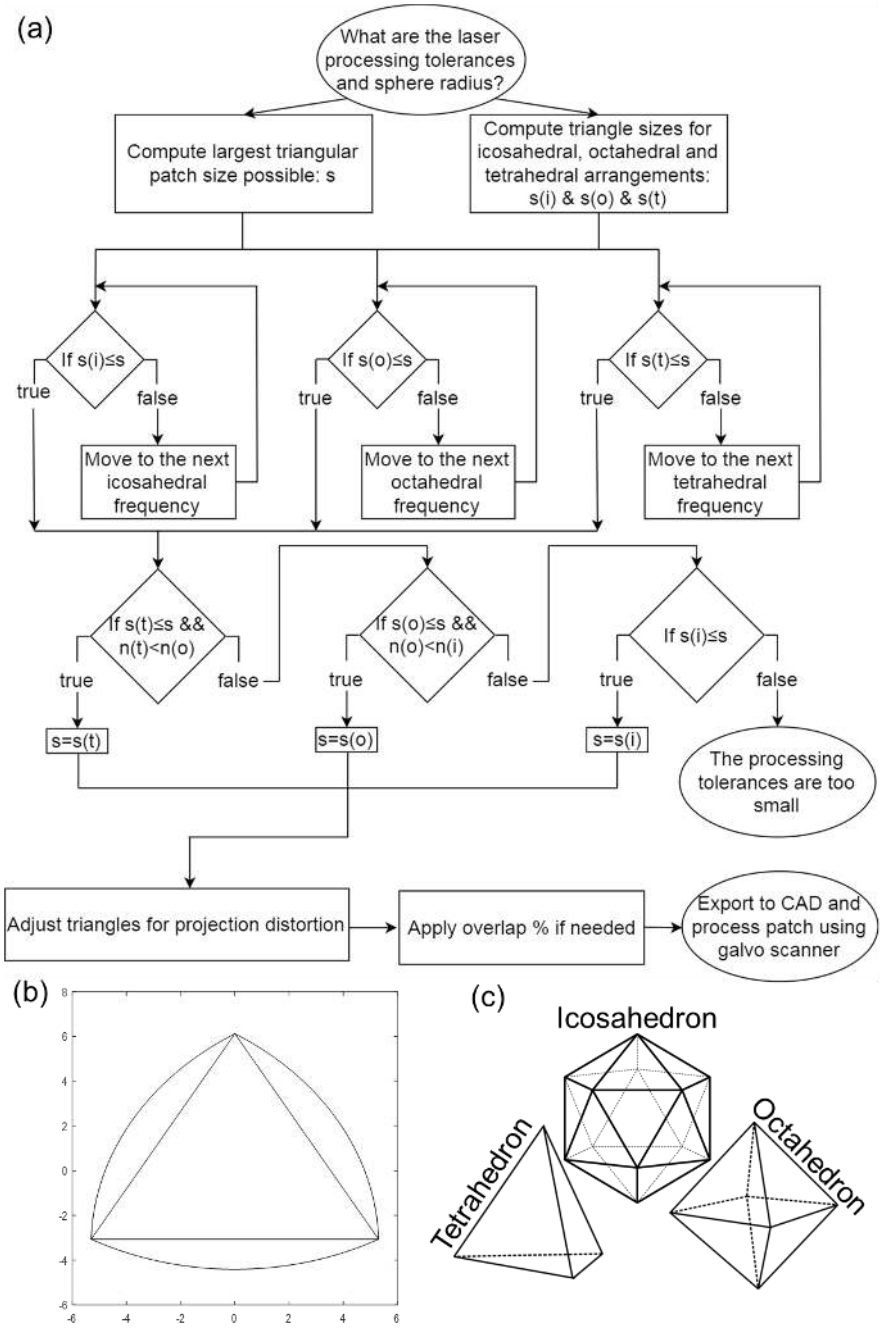

Figure 7. An overview of the tessellation method: a) the flowchart of the algorithm implemented in the MATLAB program b) an example of an output field with the projection distortions c) the examined types of geodesic polyhedra

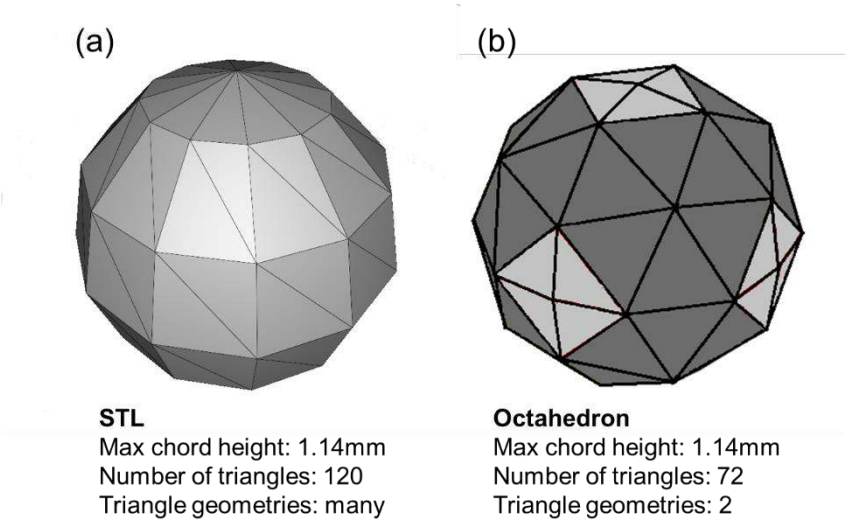

Figure 8. Comparison between STL and geodesic tessellations

3.5 Surface characterization

Topographies and surface roughness of planar and spherical surfaces were assessed using focus variation (FV) microscopy, specifically with Alicona G5 InfiniteFocus system. The surface roughness parameters were measured over a 812.173x812.173 µm area using the 20x objective with polarization and a vertical resolution of 50nm (0.075 µm smallest measurable S_a). The exposure used was 38.72 ms and the cut-off wavelength λ_c was 162.346 µm. The surface morphology was also assessed via scanning electron microscopy, specifically the Jeol JCM-6000 with EHT of 15.00kV.

4. Results and discussion

The results of the pilot implementation of the proposed methodology are presented and discussed in this section. In particular, it includes the carried-out experiments to determine the 3D tolerances of the LP and LST operations. Also, the application of the MATLAB program to generate the necessary CAD models for executing these two operations on the spherical surfaces.

4.1. Laser polishing process

The first step in applying the proposed methodology is to identify a set of optimized LP parameters for processing planar Ti-6Al-4V samples produced by LPBF. Then, they are used to study the effects of laser processing disturbances, i.e. variations of FOD and BIA, on the LP performance.

The reference LP parameters provided in Section 3.2 were used in the pilot implementation to investigate the effects of the two processing disturbances**.** First, a planar Ti-6Al-4V sample produced by LPBF was LP'd with the optimized offset and with BIA normal to the substrate surface. The roughness of the sample, i.e. S_a and S_q, was reduced from around 5.0 µm and 7.0 µm down to under 0.2 µm and 0.2 µm, respectively, resulting in a maximum improvement of 96% as shown in Figure 9.

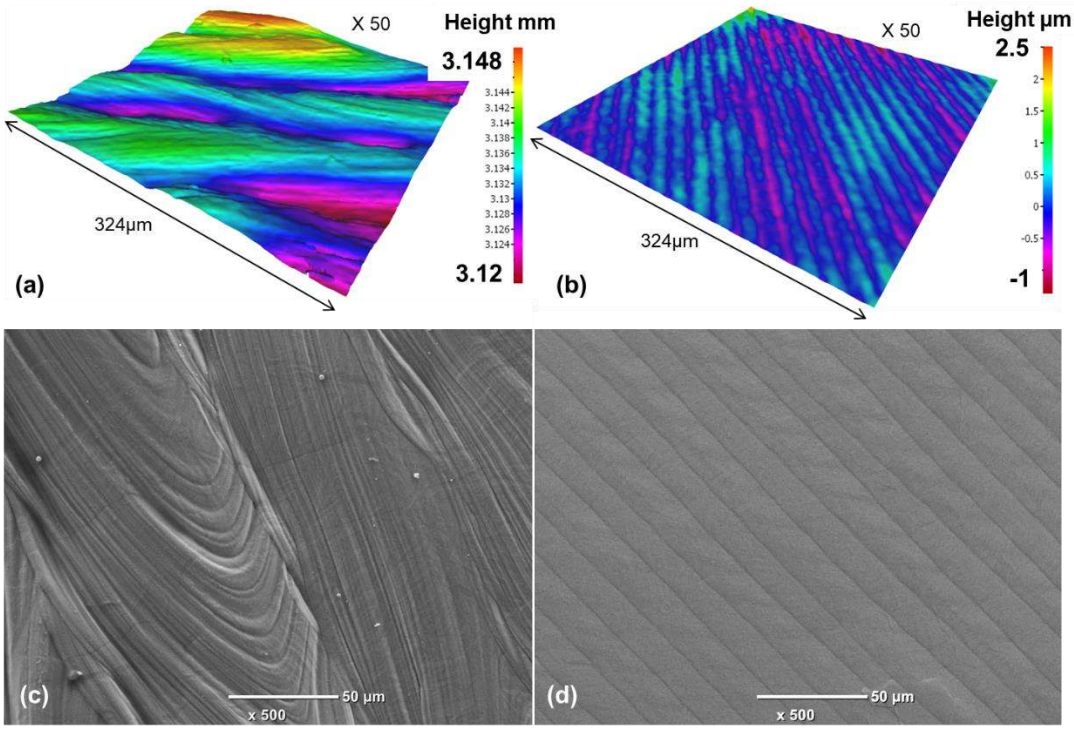

Figure 9. Laser polishing performance on a planar 3D printed Ti-6Al-4V sample a) 3D topological view of as-printed surface b) 3D topological view of polished surface (c) SEM micrograph of as-printed surface d) SEM micrograph of polished surface.

The next step was to investigate the effects of FOD and BIA separately on planar Ti-6Al-4V surfaces by using as reference the optimum LP results obtained prior.

The FOD value was varied in increments of 0.5 mm above and below the substrate surface of the planar samples and the FOD effects on the surface roughness were assessed. The measurement results obtained with FOD above and below the surface were similar and therefore only those obtained above the focal plane are discussed further. The LP results were considered acceptable when S_a was less than 0.5 µm. When the FOD was in the range from 2.5 to 3.5mm the polishing performance was tolerable, and the lowest roughness value of 0.18 µm was obtained with a FOD of 3 mm as shown in Figure 10. At a FOD of 2mm, some signs of laser ablation were observed on the surface of the Ti-6Al-4V sample, whereas at 4mm FOD, the waviness of the printed substrates was not reduced. Therefore, FOD of 3 mm with a tolerance of 0.5 mm was selected to partition and polish the fields of the printed spherical shells.

Assuming a perfect Gaussian distribution of the beam intensity, its diameter at an offset z from the focal plane can be calculated as follows [27]:

$$D(z) = D_0\sqrt{1 + (\frac{z}{z_R})^2} \qquad (4)$$

where: D_0 is the beam diameter at the focal plane and z_R the Rayleigh length. Thus, the beam spot size increases from around 80 to 140 µm when FOD is raised from 2 to 4mm,

resulting in a decrease of power density, a key laser polishing parameter, that is inversely proportional to the beam spot size by nearly a factor of 2.

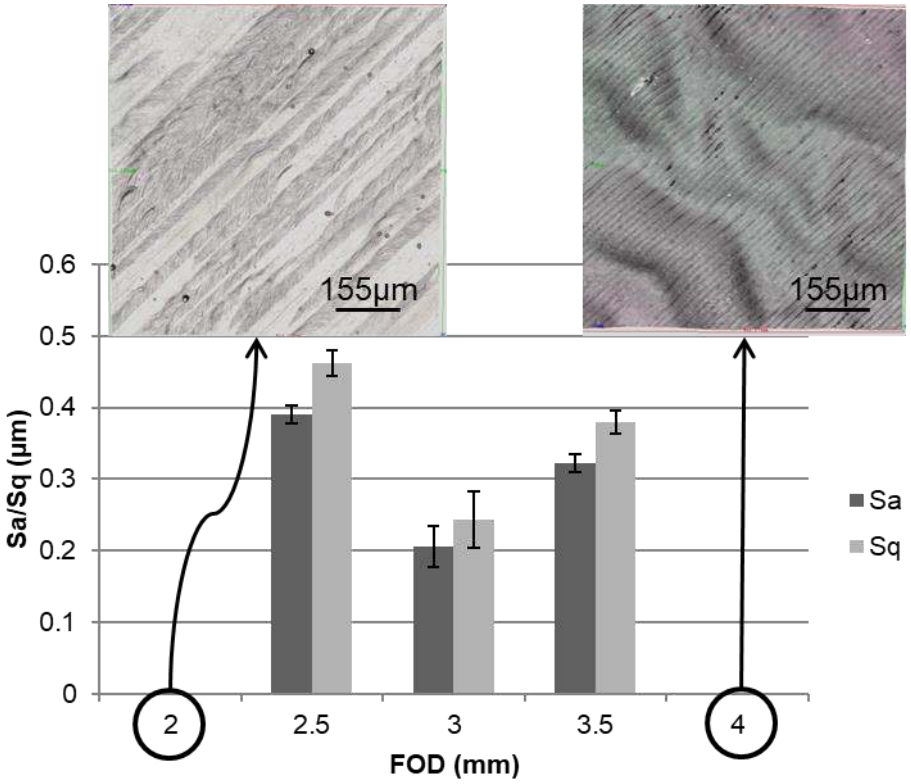

Figure 10. Effects of FOD on polishing performance
(n=3, error bars represent the standard deviation)

Next, the BIA was varied in increments of 10˚. A steady increase in surface roughness was observed with the increase of BIA as depicted in Figure 11. The polishing process was still acceptable at BIA of 40˚, however at 50˚ a sharp deterioration in the LP performance occurred, surface cracks and increased waviness were observed on the surface. At higher BIAs the Gaussian energy distribution of the beam is distorted and the pulse power density is compromised [22]. Furthermore, the material's reflectivity increases at high BIAs and thus the laser absorption is reduced [28]. Therefore, the max BIA when polishing LPBF Ti-6Al-4V should be limited to 40˚ in this setup.

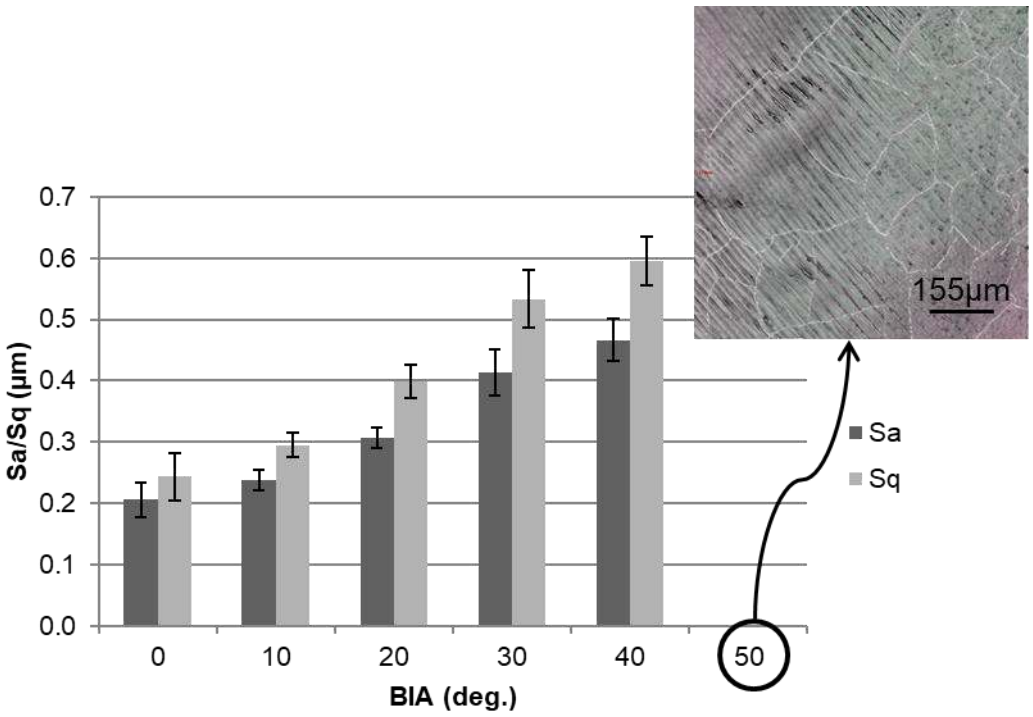

Figure 11. Effects of BIA on polishing performance
(n=3, error bars represent the standard deviation)

4.2. Laser polishing fields' stitching

The stitching areas between LP fields should be analyzed too, as they can affect the performance of the follow up LST operation and the overall part aesthetic. The surface defects in these areas can be minimized by counteracting the negative dynamics effects of the beam deflectors. In this research, the negative dynamic effects were minimized by employing a built-in software tool in the used laser processing setup [29]. However, the conducted planar LP trials revealed that there were some surface defects in spite the use of this tool at the borders between the LP fields and the un-processed surface. In particular, there were surface cracks and some material build-up near the fields' borders followed by a groove before transitioning back to the original, unprocessed surface, as depicted in Figure 12. Those are predominantly due to the flow of the molten material on the surface [15].

A representative SEM image of surface defects at the border between two adjacent LP fields without any overlapping is provided in Figure 13a. The formation of peaks and valleys between the fields was aggravated by stitching them as precisely as possible. Therefore, the use of some overlapping to minimize these defects was investigated as a potential solution.

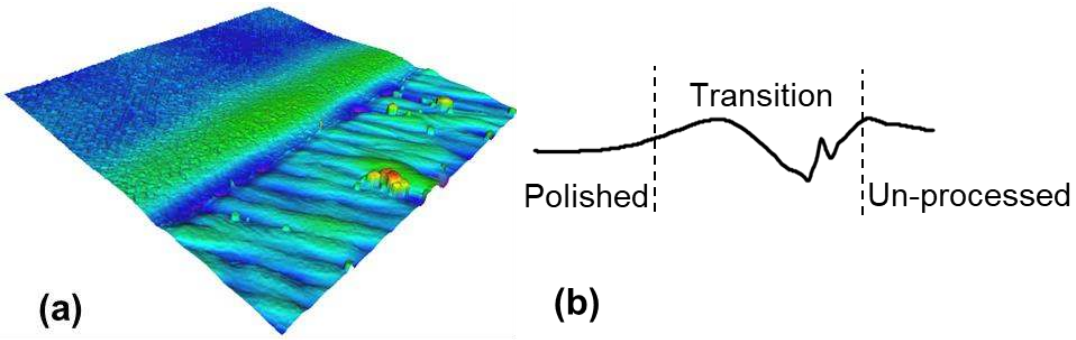

Figure 12. An analysis of the transition zone between a laser polished field and un-processed surface: a) 3D representation of the transition zone b) a representative surface profile of the transition zone obtained via FV microscopy

The level of overlapping between the LP fields was varied to investigate its impact on resulting surface morphology. LP trials of fields with varying overlapping areas were conducted while the same LP strategy, processing parameters (as given in Section 3.2) and waiting time between any two adjacent fields were used. The level of overlapping was selected to cover the material build-up at the border regions between adjacent LP fields when no overlap is applied, the width of these regions was measured to be less than 200 µm. The overlapping distance was controlled using Aerotech's PRO165LM series mechanical stages with a stated accuracy of ±1 µm.

The increase of the overlapping distance from 0 to 160 µm reduced surface cracks and the depth of the resulting 'valleys' between the LP fields and thus a smoother transition between them was achieved. In particular, the depth of the 'valleys' on the LP surfaces was measured using the FV microscope and it decreased steadily from approximately 35 µm to just under 7 µm when the overlap distance was increased from 0 to 160 µm as shown in Figure 13. Therefore, when surfaces are partitioned for LP, a controlled overlapping between the fields should be introduced to minimize any side effects, and thus achieving the smoothest possible transition between them. In this way, the uniformity of LP surfaces can be improved substantially and parts' aesthetics can be enhanced.

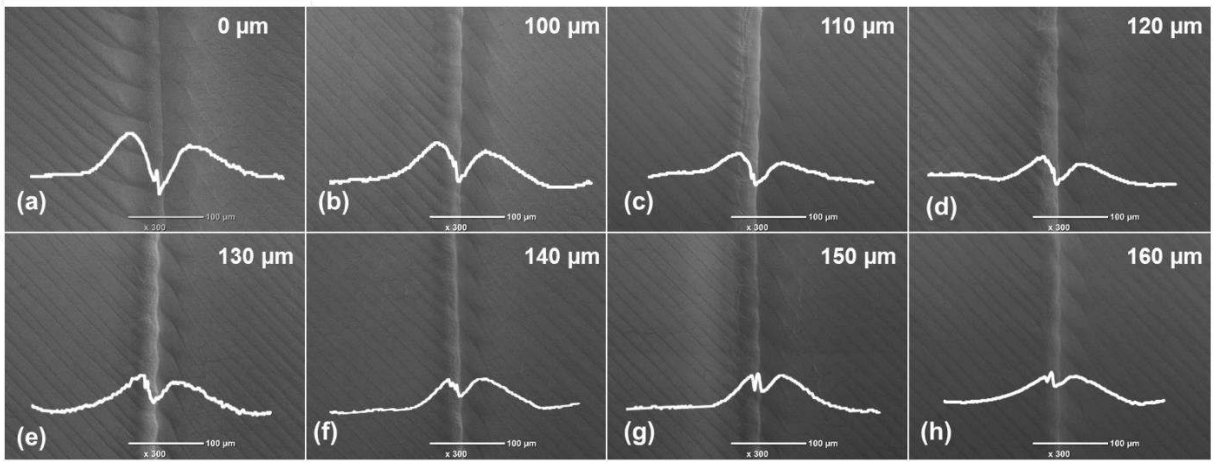

Figure 13. SEM micrographs and representative profiles of laser polished fields' borders when the overlapping distance was increased from 0 to 160 µm

Increasing the overlap distance further up to 200 μm, showed no sign of improvement to the joining process; the border area seemed more or less identical and therefore a 160 μm overlap was used in the LP operation.

4.3. Laser surface texturing of laser polished surfaces

The next step in applying the proposed methodology is to identify a set of optimized LST parameters for processing laser polished planar Ti-6Al-4V samples produced by LPBF. Again, as it was the case with the LP operation, they are used to study the effects of laser processing disturbances, i.e. variations of FOD and BIA, on the LST performance.

The reference LST parameters provided in Section 3.3 were used in this pilot implementation to investigate the effects of processing disturbances**.** In particular, the printed Ti-6Al-4V planar substrates polished using the laser parameter settings in Table 1, were successfully textured using the LST parameters provided in Table 2 when no processing disturbances are present. The substrates were fully covered with LIPSS and the preceding LP operation did not seem to affect in the LIPSS formation in any way. As expected, the resulting sub-micron ripples were perpendicular to the laser polarization vector and their periodicity was 860 ± 10nm. The ripples formed over the visible LP track lines with no apparent alterations to their morphology as can be seen in Figure 14a.

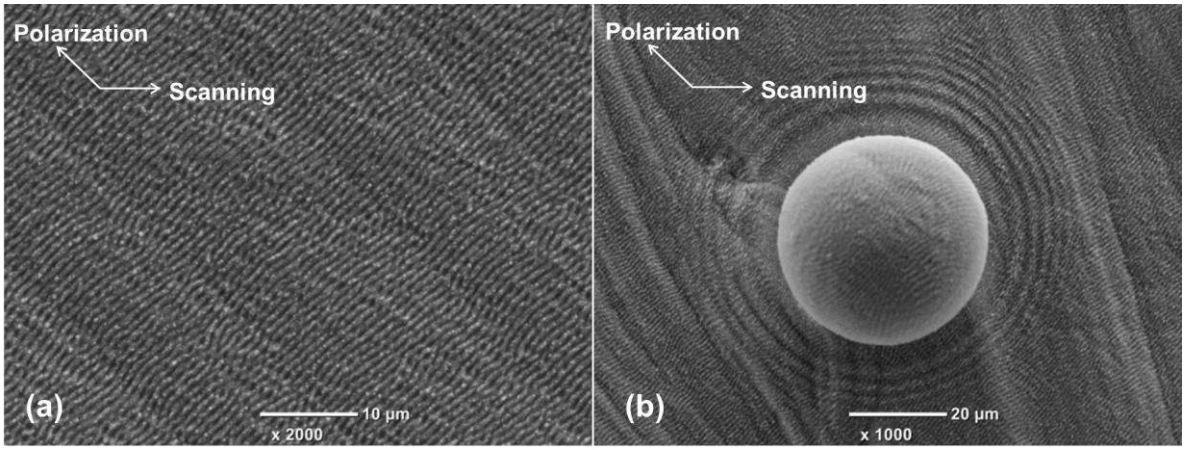

Figure 14. (a) Laser surface texturing on laser polished surface (b) Laser surface texturing on as-printed surface

The LP operation prior to LST was essential for the formation of regular and homogenous LIPSS. Any surface defects, such as sharp height variations, scratches and un-melted powder particles, as depicted in Figure 14b, can disturb the LIPSS formation and their morphology, and can thus affect their functional performance [14, 30].

The next step was to investigate the effects of the FOD and BIA separately on planar LP Ti-6Al-4V surfaces by using as a reference LST results obtained without any processing disturbances.

With the increase of FOD, the laser spot size would increase too, and thus the pulse fluence would effectively be reduced. The formation of LIPSS on surfaces requires a certain threshold fluence under which no texturing would occur. Therefore, the max acceptable FOD was determined experimentally by increasing FOD until this threshold fluence was reached on the laser polished Ti-6Al-4V substrates. In particular, the FOD was deemed acceptable if

the substrate surface was entirely covered in LIPSS. Based on the conducted LST trials on laser polished Ti-6Al-4V samples, the FOD limit was found to be 0.8 mm.

Regarding the BIA, its increase leads to an increase in the ripples' periodicity, as was already reported by other researchers [31]. For the considered texture in our experimental study, LIPSS periodicity variations were acceptable and therefore, the BIA was deemed not important. Consequently, the FOD was considered as the only limiting factor and thus used as the sole 3D processing tolerance for the LST operation on 3D surfaces.

Finally, the level of overlapping of LST fields was also investigated similarly to the LP process. However, it became immediately evident that varying the overlapping between the LST fields did not influence LIPSS formation as no discernible differences could be seen in SEM micrographs when the overlapping levels were varied. Therefore, it was concluded that overlapping between LIPSS fields was not necessary. Furthermore, the morphology of LIPSS was examined at the border area between two LP fields with a 160 µm overlap. Again, there were no alterations to their periodicity, orientation or regularity as depicted in Figure 15.

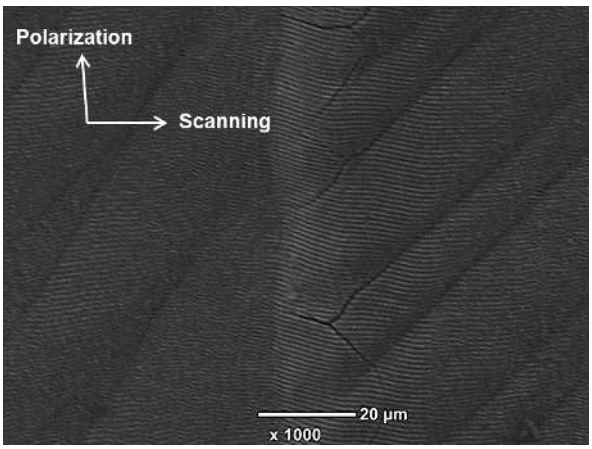

Figure 15. LIPSS over a representative border between two laser polished fields with a 160 µm overlap

4.4. Laser polishing and surface texturing of Ti-6Al-4V spherical shells

Prior to processing the spherical shells, the positional accuracy and repeatability of the manual C rotary axis to be used in the experiments, were determined by conducting some trials. In particular, equidistant crosses on the mirror finish surface of ball bearings were produced using the fs laser while repositioning them with the manual C rotary axis. The obtained actual distances between the crosses were compared with the nominal one to judge about the positioning accuracy. In addition, a second set of crosses was produced, and the displacements between the first and second set were used to assess the process repeatability. The standard deviations of those measurements were used to quantify the processing uncertainties associated with the used experimental setup. In particular, the trials were repeated 6 times and the distances between crosses were measured using the 20x objective of the FV microscope. The standard deviation of these measurements was 33 µm, both for positional accuracy and repeatability, and therefore this was considered to be the uncertainty associated with the used laser processing setup.

The MATLAB program described in Section 3.4 was used to partition and fully pre-process the CAD model of the spherical shell by using as inputs the shell diameter and the laser processing tolerances associated with LP and LST operations (see Sections 4.1 and 4.3). In particular, the spherical surface was partitioned into 80 triangular fields with an Icosahedral arrangement by inputting the LP processing tolerances of 0.5 mm and 40˚ for FOD and BIA respectively. By increasing the FOD tolerance to 0.57 mm it was possible to reduce the number of triangular fields down to 72. This was achieved at the expense of a 35 μm increase in FOD on either side of the focal plane only, which was considered an acceptable compromise to the LP process considering the significant reduction in processing time. The resulting partitioning of the spherical shell for the LP operation was comprised of only two sizes of triangular fields that formed the second sub-division (third frequency) of the octahedron with the geodesic notation $\{3,4+\}_{0,3}$.

As for the LST operation, the input for the MATLAB program was a processing tolerance of 0.8 mm for FOD and no constraints with regard to BIA, it generated the same triangular arrangement as for the LP process. Thus, both operations utilized the same geodesic arrangement while satisfying their respective processing tolerances.

Furthermore, the program applied the necessary corrections for projection distortion and added the necessary overlapping between the fields for the LP operation. In particular, considering the minimum overlapping distance of 160 μm required for the LP operation (see Section 4.2) it was necessary to adjust the triangular fields, accordingly, using the MATLAB program as described in Section 2.4. The smallest distance from the centroid to the border of the triangular patch in the generated CAD model was identified to be 1.6805 mm, and therefore the respective overlapping percentage to ensure a minimum overlap distance of 160 μm was calculated as follows:

$$\frac{0.5 \times overlap\ distance}{\min distance\ from\ centroid} \times 100 = \frac{0.5 \times 0.16}{1.6805} \times 100 = 4.76\% \quad (6)$$

Thus, taking into account the relatively small compensation required for the processing uncertainty associated with the used machine setup, in addition to the necessary overlapping of 4.76%, the adjustment applied to the fields was increased to 5% for both operations for simplicity, since overlapping did not have an effect on the LST process.

The LPBF Ti-6Al-4V spherical shells were then polished and subsequently textured using the laser processing setup shown in Figure 6, while the CAD data for the LP and LST operations was generated by applying the geodesic triangulation algorithm with the identified processing tolerances in Sections 4.1 and 4.3. To assess the LP performance, the surface roughness was measured 3 times in 3 different areas within a triangular field as shown in Figure 16b and their borders were examined (Figures 16c and 16d).

The proposed tessellation method in Section 2.2 takes into account the FOD and BIA constraints associated with the LP and LST operations, and therefore should lead to a process performance within the pre-defined limits. It is expected for the two processes to be near their limits at the vertices of the triangular fields. The obtained average S_a values on the spherical surface were 0.38, 0.42 and 0.51 μm in the areas 1, 2 & 3, respectively (Figure 16b). As expected, area 3, the closest to one of the triangle's vertices exhibited the highest S_a, just marginally higher than acceptable value of 0.5 μm. Furthermore, the roughness in area 2 was slightly higher compared to that obtained in area 1. This could be explained with

the FOD effects on the LP performance, particularly, the FOD was higher in area 2 compared with that in area 1. Overall, the LP performance on the spherical shells was slightly behind when compared to the results obtained on planar substrates, but this was expected. The higher roughness observed on the laser polished 3D surfaces could be attributed to the presence of a combined effect from both processing disturbances, i.e. FOD and BIA, while they were investigated separately in section 4.1. Another possible explanation that could have impacted the polishing results on the sphere is the laser fields' geometry. Due to the thermal nature of the ns laser polishing process, the size of the processed area directly correlates with the applied thermal load onto the surface, an important factor that impacts this polishing process based on surface re-melting [32]. In fact, smaller laser fields reduce heat dissipation from the processing area whereas larger ones stretch the temporal distances between consecutive scan lines and subsequent passes and thus allow for some cooling to occur. In the given pilot implementation, the triangular fields were comparable in size to the 3x3 mm square fields used to optimize the LP process prior in sections 4.1 and 4.2. However, if this is not the case, then some compensation should be introduced in the LP parameters to account for the discrepancy in thermal load associated with the size difference. Regardless, the LP process still performed within the set tolerable limits, especially, average S_a was below the acceptable chosen threshold value of 0.5 µm.

The borders between the LP fields were then examined by taking surface profiles. The maximum depth of the resulting 'valleys' at the borders was 8 µm and thus slightly higher compared to on the planar samples where it was less than 7 µm (Figure 16d). This can again be attributed to the presence of a combined effect and/or the different patch geometry. Still, the difference is negligible.

Finally, regarding the LST process, the triangular fields were fully covered with LIPSS and their light diffraction characteristic can be clearly seen in Figure 16a.

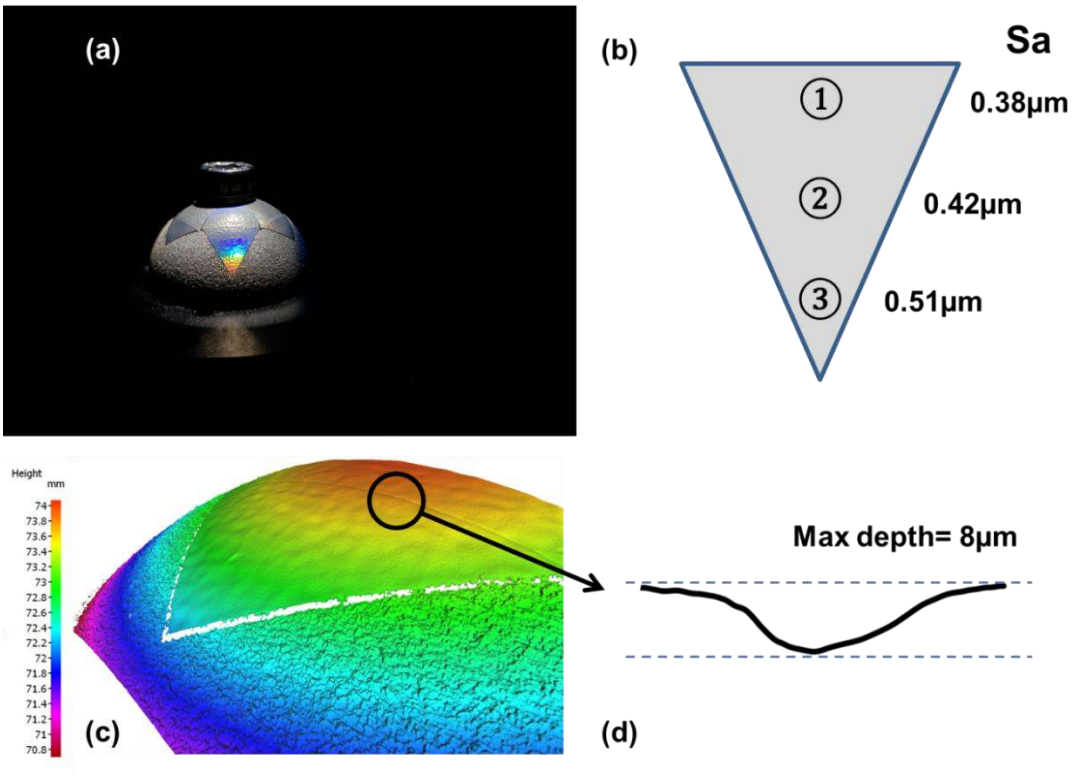

Figure 16. The results obtained on additively manufactured Ti-6Al-4V spherical shells: (a) a laser polished and textured spherical shell (b) three areas where surface roughness measurements were taken over the laser polished fields (c) 3D topological view of laser processed area (d) a representative profile scan of a border between two laser polished fields with the applied overlap

5. Conclusion

The paper demonstrates a significant development in 3D laser processing technology. Following a set of preliminary experiments, the empirical 3D limitations of a given laser process are used as input arguments to efficiently tessellate freeform surfaces. The resulting triangular partitions then serve as laser processing fields. By employing this method, processing efficiency is maximized by minimizing part repositioning, maximizing the use of fast galvo scanners, and ensuring process performance within the laser fields. In the pilot implementation, the new approach was used to successfully laser polish and texture the surface of 3D printed Ti-6Al-4V spherical shells. The presented method can be applied to any 3D part, granted the laser operation has some flexibility in terms of focal offset and beam incidence and the beam line of sight is uninterrupted. Considerations regarding patch joining and the combined effect of the beam angle of incidence and focal offset on the laser process performance should be made when using this method.

In future work, other approaches for improving the stitching quality between the triangular fields can be investigated, for example, randomizing the overlap between scanning vectors and their position in the joining area, in order to mask their presence. While the combined effect present in 3D laser processing could be measured empirically for a given laser task, greatly increasing the number of initial experiments, alternatively, modelling the beam energy distribution over the 3D part could potentially help better understand and quantify its effects.

Acknowledgment

The research reported in this paper was supported by a H2020 Factory of the Future projects, “High-Impact Injection Moulding Platform for mass-production of 3D and/or large micro-structured surfaces with Antimicrobial, Self-cleaning, Anti-scratch, Anti-squeak and Aesthetic functionalities” (HIMALAIA) and the UKIERI DST programme “Surface functionalisation for food, packaging, and healthcare applications”. The authors would like to acknowledge also the collaboration with LASEA SA, Belgium within the framework of the ESIF project “Smart Factory Hub” (SmartFub).

References

1. Javaid, M. and A. Haleem, *Additive manufacturing applications in orthopaedics: A review.* J Clin Orthop Trauma, 2018. **9**(3): p. 202-206.
2. Sing, S.L., et al., *Laser and electron-beam powder-bed additive manufacturing of metallic implants: A review on processes, materials and designs.* J Orthop Res, 2016. **34**(3): p. 369-85.
3. Szost, B.A., et al., *A comparative study of additive manufacturing techniques: Residual stress and microstructural analysis of CLAD and WAAM printed Ti-6Al-4V components.* Materials & Design, 2016. **89**: p. 559-567.
4. Lyczkowska, E., et al., *Chemical polishing of scaffolds made of Ti-6Al-7Nb alloy by additive manufacturing.* Archives of Civil and Mechanical Engineering, 2014. **14**(4): p. 586-594.
5. Ma, C.P., Y.C. Guan, and W. Zhou, *Laser polishing of additive manufactured Ti alloys.* Optics and Lasers in Engineering, 2017. **93**: p. 171-177.
6. Ezugwu, E.O. and Z.M. Wang, *Titanium alloys and their machinability—a review.* Journal of Materials Processing Technology, 1997. **68**(3): p. 262-274.
7. Wahab, J.A., et al., *Enhancing material performance through laser surface texturing: a review.* Transactions of the Institute of Metal Finishing, 2016. **94**(4): p. 193-198.
8. Shah, F.A., et al., *Laser-Modified Surface Enhances Osseointegration and Biomechanical Anchorage of Commercially Pure Titanium Implants for Bone-Anchored Hearing Systems.* Plos One, 2016. **11**(6).
9. Mariscal-Munoz, E., et al., *Osteoblast differentiation is enhanced by a nano-to-micro hybrid titanium surface created by Yb:YAG laser irradiation.* Clinical Oral Investigations, 2016. **20**(3): p. 503-511.
10. Sipe, J.E., et al., *Laser-Induced Periodic Surface-Structure .1. Theory.* Physical Review B, 1983. **27**(2): p. 1141-1154.
11. Villerius, V., et al., *Ultrashort pulsed laser ablation of stainless steels.* International Journal of Machine Tools and Manufacture, 2019. **138**: p. 27-35.
12. Lee, B.E.J., et al., *Characterization and evaluation of femtosecond laser-induced sub-micron periodic structures generated on titanium to improve osseointegration of implants.* Applied Surface Science, 2018. **441**: p. 1034-1042.
13. Cunha, A., et al., *Human mesenchymal stem cell behavior on femtosecond laser-textured Ti-6Al-4V surfaces.* Nanomedicine, 2015. **10**(5): p. 725-739.
14. Batal, A., et al., *Effects of laser processing conditions on wettability and proliferation of Saos-2 cells on CoCrMo alloy surfaces*, in *Advanced Optical Technologies*. 2019.
15. Bhaduri, D., et al., *Laser polishing of 3D printed mesoscale components.* Applied Surface Science, 2017. **405**: p. 29-46.
16. Marimuthu, S., et al., *Laser polishing of selective laser melted components.* International Journal of Machine Tools & Manufacture, 2015. **95**: p. 97-104.
17. Karoussis, I.K., et al., *Nd:YAG laser radiation (1.064 nm) accelerates differentiation of osteoblasts to osteocytes on smooth and rough titanium surfaces in vitro.* Clin Oral Implants Res, 2017. **28**(7): p. 785-790.
18. Yung, K.C., et al., *Laser polishing of additive manufactured CoCr alloy components with complex surface geometry.* Journal of Materials Processing Technology, 2018. **262**: p. 53-64.
19. Cuccolini, G., L. Orazi, and A. Fortunato, *5 Axes computer aided laser milling.* Optics and Lasers in Engineering, 2013. **51**(6): p. 749-760.
20. Jiang, M., et al., *Large scale layering laser surface texturing system based on high speed optical scanners and gantry machine tool.* Robotics and Computer-Integrated Manufacturing, 2017. **48**: p. 113-120.
21. Diaci, J., et al., *Rapid and flexible laser marking and engraving of tilted and curved surfaces.* Optics and Lasers in Engineering, 2011. **49**(2): p. 195-199.

22. Wang, X.Z., et al., *Study of laser precision ablating texture patterns on large-scale freeform surface.* International Journal of Advanced Manufacturing Technology, 2017. **92**(9-12): p. 4571-4581.
23. Stroud, I. and P.C. Xirouchakis, *STL and extensions.* Advances in Engineering Software, 2000. **31**(2): p. 83-95.
24. Dimitrov, D., et al., *Investigating the achievable accuracy of three dimensional printing.* Rapid Prototyping Journal, 2006. **12**(1): p. 42-52.
25. Giorleo, L., E. Ceretti, and C. Giardini, *Ti surface laser polishing: effect of laser path and assist gas.* 9th Cirp Conference on Intelligent Computation in Manufacturing Engineering - Cirp Icme '14, 2015. **33**: p. 446-451.
26. Wenninger, M.J., *Spherical models*. 1979, Cambridge Eng. ; New York: Cambridge University Press. xii, 147 p.
27. Meschede, D., *Optics, Light, and Lasers: The Practical Approach to Modern Aspects of Photonics and Laser Physics.* Optics, Light, and Lasers: The Practical Approach to Modern Aspects of Photonics and Laser Physics, 2017: p. 1-528.
28. Overmeyer, L., et al., *Laser patterning of thin film sensors on 3-D surfaces.* Cirp Annals-Manufacturing Technology, 2012. **61**(1): p. 215-218.
29. Penchev, P., et al., *Generic software tool for counteracting the dynamics effects of optical beam delivery systems.* Proceedings of the Institution of Mechanical Engineers Part B-Journal of Engineering Manufacture, 2017. **231**(1): p. 48-64.
30. Reif, J., O. Varlamova, and F. Costache, *Femtosecond laser induced nanostructure formation: self-organization control parameters.* Applied Physics a-Materials Science & Processing, 2008. **92**(4): p. 1019-1024.
31. Prokhorov, A.M., et al., *Excitation and Resonant Transformation of a Surface Electromagnetic Wave during Irradiation of a Solid by High-Power Laser Radiation.* Kvantovaya Elektronika, 1983. **10**(5): p. 906-912.
32. Deng, T., J. Li, and Z. Zheng, *Fundamental aspects and recent developments in metal surface polishing with energy beam irradiation.* International Journal of Machine Tools and Manufacture, 2020. **148**: p. 103472.